ACS APPLIED MATERIALS & INTERFACES

Research Article

www.acsami.org

# Passivation Dynamics in the Anisotropic Deposition and Stripping of Bulk Magnesium Electrodes During Electrochemical Cycling

David J. Wetzel,[†,‡] Marvin A. Malone,[†,‡] Richard T. Haasch,[§] Yifei Meng,[§,⊥] Henning Vieker,[∥] Nathan T. Hahn,[#] Armin Gölzhäuser,[∥] Jian-Min Zuo,[§,⊥] Kevin R. Zavadil,[#] Andrew A. Gewirth,[‡] and Ralph G. Nuzzo*[,‡]

[‡]Department of Chemistry, [§]Frederick Seitz Materials Research Laboratory, and [⊥]Department of Materials Science and Engineering, University of Illinois, Urbana, Illinois 61801, United States

[∥]Fakultät für Physik, Universität Bielefeld, Universitätsstr.25, D-33615 Bielefeld, Germany

[#]Sandia National Laboratories, Albuquerque, New Mexico 87185, United States

Supporting Information

**ABSTRACT:** Although rechargeable magnesium (Mg) batteries show promise for use as a next generation technology for high-density energy storage, little is known about the Mg anode solid electrolyte interphase and its implications for the performance and durability of a Mg-based battery. We explore in this report passivation effects engendered during the electrochemical cycling of a bulk Mg anode, characterizing their influences during metal deposition and dissolution in a simple, nonaqueous, Grignard electrolyte solution (ethylmagnesium bromide, EtMgBr, in tetrahydrofuran). Scanning electron microscopy images of Mg foil working electrodes after electrochemical polarization to dissolution potentials show the formation of corrosion pits. The pit densities so evidenced are markedly potential-dependent. When the Mg working electrode is cycled both potentiostatically and galvanostatically in EtMgBr these pits, formed due to passive layer breakdown, act as the foci for subsequent electrochemical activity. Detailed microscopy, diffraction, and spectroscopic data show that further passivation and corrosion results in the anisotropic stripping of the Mg {0001} plane, leaving thin oxide-comprising passivated side wall structures that demark the {0001} fiber texture of the etched Mg grains. Upon long-term cycling, oxide side walls formed due to the pronounced crystallographic anisotropy of the anodic stripping processes, leading to complex overlay anisotropic, columnar structures, exceeding 50 $\mu$m in height. The passive responses mediating the growth of these structures appear to be an intrinsic feature of the electrochemical growth and dissolution of Mg using this electrolyte.

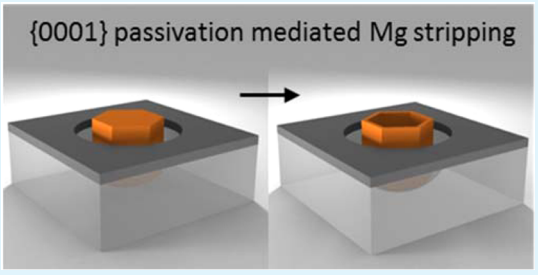


**KEYWORDS:** *rechargeable magnesium battery, magnesium anode, passivation, corrosion, columnar growth*

## 1. INTRODUCTION

Recently, there has been an accelerated push toward the development of rechargeable batteries that use bulk metal anodes.[1−7] The use of metal anodes in energy-storage devices is seen as being advantageous due in part to their high theoretical energy densities and capacities. Various performance-related issues, however, have limited the development of market-ready, bulk metal-anode-based rechargeable batteries. Lithium (Li) metal, for instance, has received significant attention in research, but to date viable technologies have yet to emerge due to battery failures that occur from the formation of Li dendrites that grow out from the metal anode surface as a result of repetitive charging and discharging.[8] Research into the causes and strategies for the elimination of Li metal dendrites is a subject of ongoing work in the field.[9−13]

Because of its physical and chemical properties, magnesium (Mg) has been considered as an alternative anode to Li metal, especially for the case of rechargeable batteries for electric vehicles. Compared to Li, Mg is divalent (with a theoretical volumetric capacity of 3832 versus 2062 mAh $cm^{-3}$), more abundant, less toxic and, most importantly, less susceptible to dendritic growth. Metallic Mg is highly reactive, however and is thus susceptible to passivation, which is problematic for its use as an electrode. When exposed to air, Mg forms a surface layer consisting of atmospheric contaminants, most notably oxide and hydroxide, although with proper surface preparation this surface film can be reduced or eliminated.[14] Nevertheless, even if the initial oxide layer is removed, Mg still can be passivated from species developed as a consequence of electrochemical activity. The current literature suggests the reactivity of the electrolyte solvent plays a central role to this end. Such features of the reactivity of Mg have limited the use of nonaqueous solvents to primarily ethers.[15]

Received: May 23, 2015
Accepted: August 10, 2015
Published: August 10, 2015





DOI: 10.1021/acsami.5b04487
ACS Appl. Mater. Interfaces 2015, 7, 18406−18414

Such issues notwithstanding, there has been a marked increase in work focused on the study of Mg rechargeable batteries.[16−28] The majority of this work has been focused on the discovery and characterization of novel nonaqueous electrolytes with large electrochemical windows. There has been some consideration of corrosion given in studies of nonaqueous magnesium battery chemistries, work that has generally focused on degradation of the current collector and other system components. This work has shown that Mo is stable to high potentials whereas stainless steel is not, implying stainless steel components high in Mo content may yield stable Mg battery current collectors and casings.[20,29] Although the stability of nonactive components toward corrosion is important for Mg batteries, the study of passivation and corrosion of Mg itself is also important for understanding Mg self-discharge and losses in Coulombic efficiency. Hardly any work related to Mg rechargeable batteries has examined the morphology of bulk Mg anodes as result from extended electrochemical processing in nonaqueous solutions, except to note that Mg tends to form strongly passivated surfaces using electrolyte mimics of traditional Li-ion batteries.[14]

In this paper, we examine the morphologies of Mg anodes after polarization to dissolution potentials, as well as cyclic potential steps, in order to develop insights into the passivation dynamics and electrochemically mediated corrosion processes of Mg as occur in Grignard-based electrolytes and how these processes might impact the viability of Mg as an energy storage material. We note that electrolyte examined here is a simple, and arguably prototypical, electrolyte system for nonaqueous Mg electrodeposition. The modification of this electrolyte through the addition of Lewis acids is also known to engender important impacts on performance, albeit with some concern as to the sensitivity of these more complex compositions to as yet poorly understood features of electrolyte synthesis procedures. The latter concern is one that motivated our selection of the highly reproducible, widely studied ethylmagnesium bromide electrolyte in THF as the system for study in this work. We show that upon extensive cycling the inherent dynamics of the processes involved are distinguished by strong crystallographic anisotropies and passive film formation, particularly during Mg stripping, that lead to the growth of anisotropic columns of Mg that could lead to battery failures not unlike those that result from Li dendrites.

## 2. EXPERIMENTAL DETAILS

Ethylmagnesium bromide, 1.0 M in tetrahydrofuran (EtMgBr-THF), the electrolyte used for all electrochemical experiments, was purchased from Sigma-Aldrich and used with no further preparation. All electrochemical experiments were carried out in an argon-filled MBRAUN LABstar glovebox. Electrochemical experiments were performed using either a CH Instrument 650 B or 660 D analyzer/workstation. Electrochemical cell components were acid washed, rinsed with Milli-Q water, and oven-dried before each use. Magnesium foil (GalliumSource, LLC), 99.95% and 0.05 mm thick, was used as the working electrode for most experiments. Immediately prior to each experiment a new piece of Mg foil was polished with 421 polishing compound, a felt pad, and rotary tool (all purchased from Dremel) inside the glovebox, then washed with THF and wiped with a cloth to remove excess polishing compound. Although several chemical polishing methods were attempted, mechanical polishing inside the glovebox resulted in the best finish and thinnest oxide layer on Mg (as confirmed by electrochemical and microscopy measurements). For all experiments, the counter and reference electrodes used were similarly polished strips of Mg ribbon.

The scanning electron microscope (SEM), X-ray diffraction (XRD), X-ray photoelectron spectroscopy (XPS), and focused ion beam (FIB) instrumentation used in this work are located at the Frederick Seitz Materials Research Laboratory (FS-MRL) on the campus of the University of Illinois at Urbana−Champaign and described at mrl.illinois.edu. The helium ion microscope (HIM) images were taken at Bielefeld University in Bielefeld, Germany (see below).

A Hitachi S4700 high resolution SEM and a JEOL 7000F analytical SEM were used in the collection of SEM images. After the completion of each experiment, the Mg foil was rinsed with THF and allowed to dry inside the glovebox after which it was transferred to the SEM. During transfer to the SEM the Mg foil is exposed to air therefore, in order to limit this exposure, Mg foils were transferred immediately before analysis.

A PANalytical Philips X'pert MRD system equipped with a Cu K-$\alpha$ source at 0.15418 nm was used for X-ray diffraction experiments. A polycrystalline Mg substrate was purchased from MTI Corporation and used as a reference. XRD 2-theta scans were taken at a scan rate of 2° $min^{-1}$ for both the Mg foil and polycrystalline substrate. Pole figures of the (002) diffraction line were also obtained for both samples of Mg. XRD results were analyzed using JADE XRD analysis software.

A Physical Electronics PHI 5400 equipped with a Mg source and a pass energy of 35.75 eV, was used to obtain high resolution XPS results for polished, stripped, and cycled Mg foils. Electrochemical experiments were conducted inside the glovebox after which, the foils were rinsed with THF and then immediately placed within an XPS transfer vessel. The XPS vessel was then doubly sealed in resealable bags and transported directly from the glovebox to the XPS instrument, where the vessel works as a load lock. The transfer procedure was done to keep the samples from being exposed to air. The samples were electrically grounded, and binding energies were calibrated using the Ag 3d5/2 peak at 368.06 eV (+0.24 eV) measured from a reference foil within the vacuum chamber.

A FEI Helios 600i focused ion beam (FIB) with a gallium ion source was used to mill structures in preparation for helium ion microscope imaging. The HIM images were taken with a Carl Zeiss Orion Plus helium ion microscope operating with an accelerating voltage of about 39.5 kV and a current of about 0.4 pA. Sample distance was 11 mm with a spot size of 10 $\mu$m and each image used averaging of 32 lines with a dwell time of 1 $\mu$s per pixel.

## 3. RESULTS AND DISCUSSION

Figure 1a shows the current−time transients (solid traces) obtained from three Mg foil working electrodes stepped from open circuit potential (approximately 50 mV vs Mg) to potentials held at 500, 700, and 900 mV in a 1.0 M solution of EtMgBr in THF for 1800 s. The potentiostatic stripping experiments highlight the initial state characteristics of the anode surface and maintain a surface at constant potential in order to evaluate the relative contribution of thermodynamic and kinetic contributions to stripping. Current−time transients of electrochemically mediated metal dissolution have been used previously to elucidate the relative kinetic and thermodynamic contributions to such processes for Cu in an aqueous electrolyte system.[30] In a similar vein, Souto et al. used nucleation and growth models to characterize the potentiostatically controlled dissolution of a Cu electrode, including above the potential at which the passive film breaks down, $E_b$, where contributions to the current density are controlled by a mixture of kinetics and diffusion. The most important point for the discussions that follow is that above $E_b$, Souto et al. observe a Cu corrosion process dominated by pit corrosion. It is observed, based on an inspection of the data presented in Figure S1, that a freshly polished Mg foil in EtMgBr-THF has an apparent $E_b$ of about 250 mV (1st cycle electrodissolution overpotential due to the initial oxide layer); because we are


DOI: 10.1021/acsami.5b04487
ACS Appl. Mater. Interfaces 2015, 7, 18406−18414

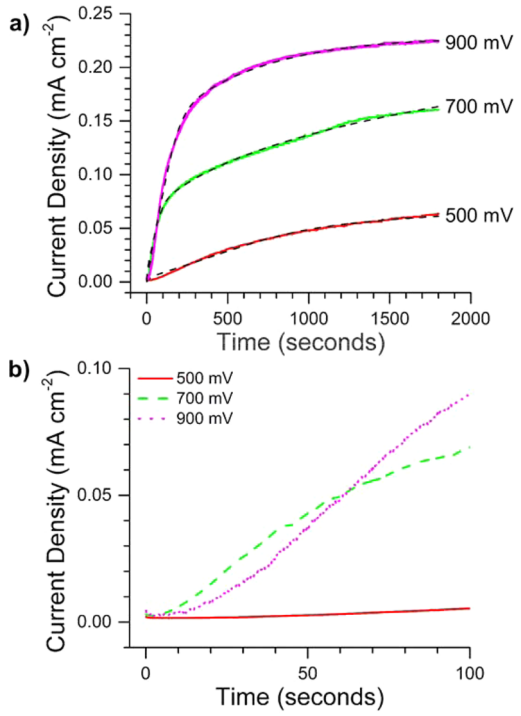


**Figure 1.** Current−time transients of polished Mg foils in EtMgBr-THF at three different dissolution potential holds of (a) 500, 700, and 900 mV for 30 continuous minutes (dashed lines represent fitting results). (b) Magnification of the region between 0−100 s in a. Counter and reference electrodes were polished strips of Mg ribbon.

above this potential for the applied potentials used for Figure 1a, it is likely that the currents seen there are ones lying in the mixed kinetic and diffusion controlled regime. Although this aqueous Cu chemistry is not fully analogous to the nonaqueous Mg electrodissolution system examined here, the general parametrization of the model used to describe it is. With this assumption, then, we fit the experimental data in Figure 1a (dashed traces) using the following general current equations as have been established for the dynamics of dissolution nucleation and growth

$$j_t = j_c + j_{d'} \quad (1)$$

$$j_c = P_4[1 - \exp(-P_5 t^2)] \quad (2)$$

$$j_{d'} = P_6 t^{-1/2}[1 - \exp(-P_7 t)] \quad (3)$$

The current response is related to the kinetic term, $j_c$, and the diffusion term, $j_{d'}$. The parameters $P_4$ and $P_5$ are apparent rate constants for pit growth. The parameters $P_6$ and $P_7$ contain the term for the diffusion coefficient of Mg ions in solution. These parameters also contain constants and properties of Mg and are fully addressed in the Supporting Information and ref 30. As shown in the work done by Souto et al., the kinetic term models the pit growth and nucleation and the diffusion term models the metal dissolution through a passive film, which suggests that the response of the Mg metal to the potentials applied in Figure 1 is the formation of pits with subsequent Mg dissolution mediated through a passive film. We cannot at present interpret these fitting parameters microscopically in terms of the precise chemical speciations/atomic structures that underpin the complex dynamical attributes (e.g., pit nucleation) evidenced in this electrochemistry, but simply note that they establish a general scaling well modeled in this way and further accord with the experimental results shown below. The fitted parameters for the transient models are provided in Table S1. As noted, the best fits were achieved when the total contribution to the current included both the kinetic and diffusion controlled transient models. Though the fact remains that Mg dissolution behaviors are not entirely understood, the goodness of fit of these models to our experimental data may supply a fundamental understanding of the dynamics involved in the dissolution of Mg in a nonaqueous electrolyte.

The data in Figure 1b present an expanded view of the current density measured from 0−100 s for each of the three applied potentials examined. These data show that, during each potential hold, there appears to be a period of quiescence—a time before substantial current begins flowing. This period appears to be greatest for the lowest magnitude potential step (500 mV) and approximately the same for the two higher overpotentials. These features have the functional form of a pitting corrosion process, where the initial induction time arises as an inherently stochastic process.[31] The fact that the initial current flow at the first potential step is not linearly correlated with the applied potential is indicative of attributes of compositional/structural complexity present in the residual oxide film left on the Mg surface by the polishing step used to activate it.[30] The data taken together suggest that polarization of the Mg foil working electrode toward dissolution potentials leads to local failures of the surface layer, leading to dissolution at sites exposed on the Mg surface. The microscopy data presented and discussed below affirms this latter point and the suitability of the functional form of the models used to quantify the potential step data of Figure 1.

The micrographs shown in Figure 2 are SEM images of three exemplary Mg metal foils following emersion during potential step experiments at three increasing potentials in a manner similar to that described for Figure 1. These images show that numerous and widely dispersed pits are present on each of the

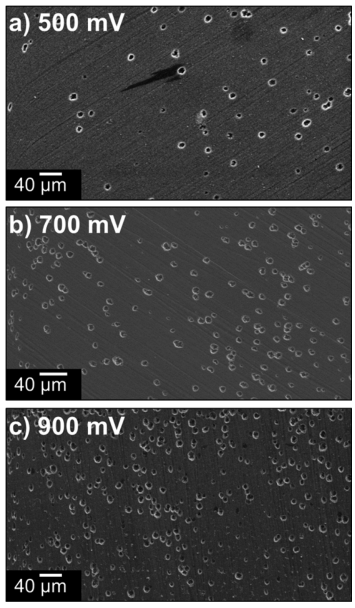


**Figure 2.** SEM images of Mg foil working electrodes after 30 continuous minutes of stripping in EtMgBr-THF at (a) 500, (b) 700, and (c) 900 mV. Counter and reference electrodes were polished strips of Mg ribbon.


DOI: 10.1021/acsami.5b04487
ACS Appl. Mater. Interfaces 2015, 7, 18406−18414

Mg foils. More importantly, a quantitative analysis of the data shows that the magnitude of the anodic potential step correlates with both the areal density of pits formed and the magnitude of the currents that flow. These features, as well as the relatively comparable dimensions of the pits, supports a model of pitting dynamics emphasizing the strong impacts of potential upon pit nucleation, yet diffusion control of their growth (Figure S2). When taken together, these data clearly reveal pitting dynamics mediate the metal dissolution and highlights a morphological embodiment for the induction time effects seen in Figure 1. It can also be seen in Figure 2 that the pits are weakly aligned with the grooves created by the polishing process. An exemplary sample with pits even more strongly aligned with the polishing defects is shown in Figure S3, along with the Fast Fourier Transform of the corresponding micrograph that shows a high intensity line perpendicular to the grooves in the original micrograph, a result strongly indicating that the pits are both parallel to the grooves and have irregular spacings. We also found at the macro scale that pits can be formed clustered in regions of higher mechanical stress, such as the area near the O-ring or regions where the foil was buckled. This suggests that a more favorable path to film breakdown occurs in regions of thinner, or less-protecting films (e.g., as due to surface defects), or where strain induced failures may exist. It has been noted in the literature that other magnesium electrolyte systems show localized regions of breakdown that increase with the anodic current density.[32]The potentiostatic stripping experiments highlight the initial state characteristics of the anode surface and maintain a constant potential surface when passivation breakdown occurs. As we show below, repeated potentiostatic stripping and deposition cycles can mitigate such sample-preparation history dependences but with the caveat that crystallographic dependences are enhanced by the inherent electrochemical reaction dynamics of this system.

The temporal evolution of the electrochemical cycling behavior of bulk Mg electrodes is illustrated in the data presented in Figure 3. Figure 3a gives plots of the electrochemical data obtained from cycling at three different limiting potential ranges: (a) slightly past $E_b$; (b) moderately into the mixed control region; and (c) at a high overpotential. The dash trace is for an electrode cycled between ∓300 mV, in which the potential was first held at −300 mV for 15 min and then switched to +300 mV for 15 min, repeating for 10 cycles. The same cycling procedure was used for the ±500 mV (solid trace) and ±700 mV (dash dot trace) cases shown in the figure. In a manner similar to what is observed in Figure 1, the current density seen in both the anodic and cathodic potential steps increases with the magnitude of the potential applied (versus a Mg reference). The data in Figure 3b plots the ratio of the integrated area for the deposition to that of dissolution step for each of the 10 cycles (presented as a percentage). It should be noted that for all but one cycle, dissolution is favored. In fact, for the ±300 mV and ±700 mV cases, dissolution is moderately more dominant than deposition for the first few cycles. The origin of this asymmetric current scaling is not completely understood. It has been observed by others that, unless the Mg metal surface is activated in the electrolyte, it will be covered in a passivating film composed of environmental contaminants[14] and though deposition is not completely blocked, it is hindered by this film. It is also known that in aqueous systems electropositive metal impurities within the Mg metal can greatly perturb the electrodynamical and chemical behaviors of a Mg electrode.[33] The atomistic features of these impacts are

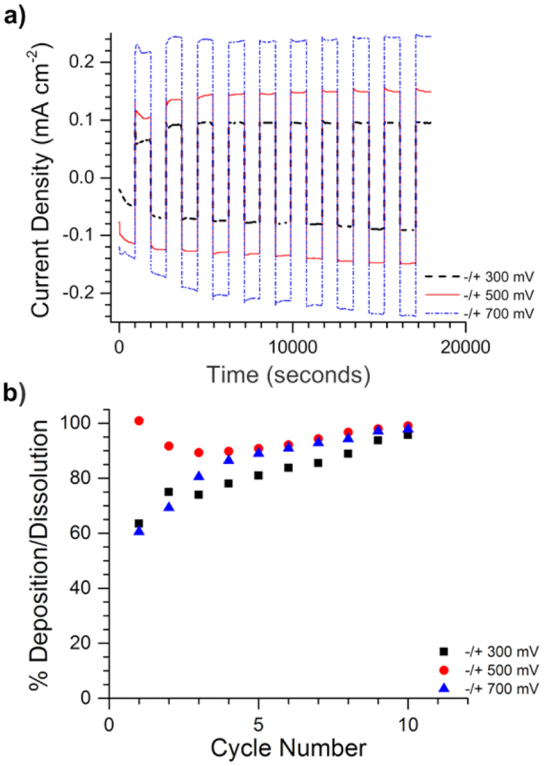


**Figure 3.** Electrochemical results from potentiostatic deposition/dissolution cycling of polished Mg foils in EtMgBr-THF. (a) deposition/dissolution cycling data for 10 cycles (15 min per half cycle) at three different potentials: ±300 mV (dash); ±500 mV (solid); ±700 mV (dash-dot). (b) Plot of the deposition/dissolution ratio presented as a percentage for ±300 mV (square); ± 500 mV (circle); ±700 mV (triangle). Counter and reference electrodes were polished strips of Mg ribbon.

not completely understood at this time. We note that it seems likely that such impurity mediated dynamics will be important for nonaqueous electrolytes as well. Even so, in the present case it remains true that the time-based measure always (with one exception) more efficiently removes Mg from the bulk anode than the deposition step adds to it for the initial cycles. The data discussed in the sections that follow suggest an explicit mechanism responsible for the more facile dissolution dynamics this rate/property correlation reveals.

The data presented in Figure 4a−c are SEM images measured for electrodes cycled at the different potential ranges after the completion of 10 full deposition/dissolution cycles. These data establish that variations in the potential produce different surface morphologies. In each case, albeit with different scales of texturing, the cycling leads to the occurrence of anisotropic Mg structures on the surfaces of the bulk electrodes. Although other structures are formed, many of the structures evidenced suggest an anisotropic pattern of growth/etching of a specific preferred orientation of hexagonal close packed (hcp) Mg grains. This finding has literature precedent in that Hill et al. observed that, under specific conditions in ether solvents containing alkyl halides, a major fraction of the pits formed on Mg metal are anisotropically etched when an {0001} oriented single crystal was used.[34] The crystallographic texture of the foil samples was examined for this reason; X-ray diffraction studies (Figure S4) show that the Mg foils used for our experiments are in fact preferentially oriented along the {0001} direction. As the data in Figure 4 illustrate, the


DOI: 10.1021/acsami.5b04487
ACS Appl. Mater. Interfaces 2015, 7, 18406−18414

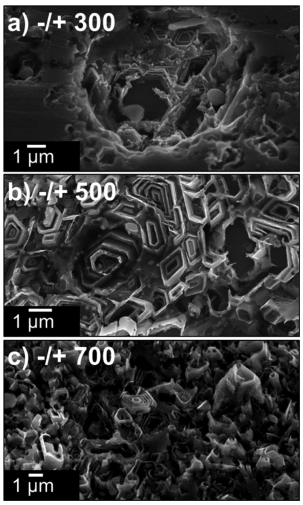


**Figure 4.** SEM images of each Mg foil working electrode after the completion of the 10 cycles for each of the experiments presented in Figure 3a; (a) ±300, (b) ±500, and (c) ±700 mV.

anisotropy that occurs after multiple cycles, after ending at the dissolution potential limit, is broadly distributed across the sample surface and comprise mainly the walls of Mg crystallites deposited with a preferred {0001} oriented texture. Geometric analysis of the structures seen in Figure 4b produces angles of 63.2° ± 4.9 and 121.5° ± 6.9, confirming roughly vertically aligned (and oblately presented) {0001} hexagonal crystals typical of an hcp lattice. In fact, the quasi-hexagonal morphology deposits are the only anisotropic texture observed, regardless of the order of the potential holds, galvanostatic vs potentiostatic cycling, or even substrate texture (Figures 5–7). Others have observed dissolution differences between planes of magnesium.[35−39] Liu et al. suggested that the activation energy of dissolution increases as the packing density of the plane increases for the hexagonal close-packed (hcp) magnesium.[36] Planes perpendicular to the {0001} basal plane, however, have lower packing densities and by this model should have a more favorable dissolution. In point of fact, the literature[35,37] contains some contradictions regarding the dissolution behaviors of the {0001} plane of Mg. Song et al.[37] observed that in 0.01 M NaCl the {0001} plane is most resistant to dissolution, yet McCall et al.[35] observed that in 0.01 M NaCl/0.0001 M dichromate solution the {0001} plane is the least resistant when compared to low-index prismatic planes (e.g., the {10−10} plane). Song et al. proposed that this contrast is due to the fact that growth of surface films can vary markedly on the different planes and also vary in different electrolytes.[37] We believe the current data support this picture of corrosion due to halide species and that the structures observed upon cycling likely result from passive films that vary in structure for the different Mg hcp planes, a factor resulting in both an anisotropic stripping and subsequent replating of the Mg. Logical inferences suggest an oxide speciation is likely for the passive films that mediate this rate-structure correlation.

To test this assumption, we determined the surface speciation of three different Mg foil samples by use of XPS. Plotted in Figure 5 are the core level data measured in the O(1s), Br(3d), and the Mg(2p) core-level binding energy regions, here recorded for a polished Mg foil (p), a Mg foil working electrode stripped at +500 mV for 30 min (s), and a Mg foil working electrode after 10 cycles at ±500 mV with the

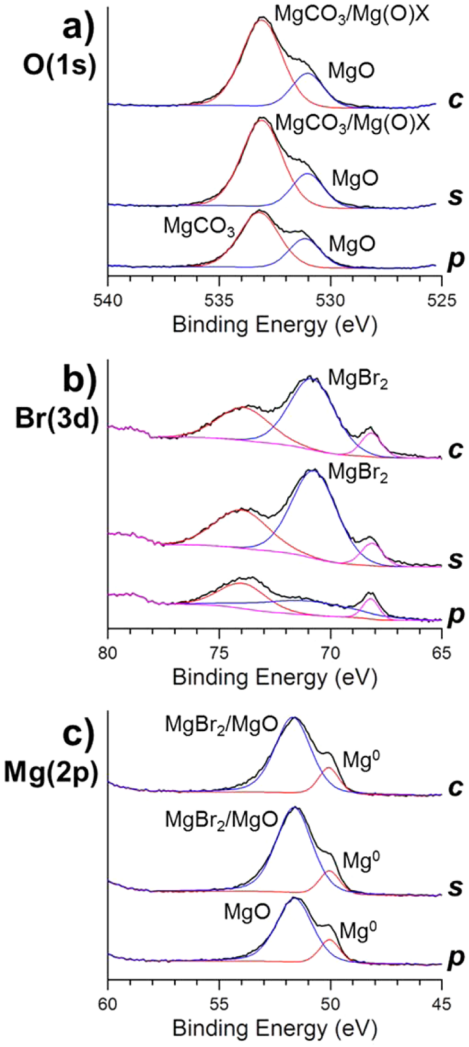


**Figure 5.** Plots of the XPS results for polished Mg foils after different electrochemical processes: (p) polished, no electrochemistry, (s) stripped at +500 mV for 30 min in EtMgBr-THF, and (c) 10 potentiostatic deposition/dissolution cycles at ∓500 mV (15 min per half cycle) in EtMgBr-THF. Plot of binding energies in the ranges of (a) oxygen (1s), (b) bromine (3d), and (c) magnesium (2p) are presented. For electrochemical processes, the counter and reference electrodes were polished strips of Mg ribbon.

cycles terminated at the anodic potential limit (c). In order to minimize exposure to air, the Mg foils were transferred to the XPS instrument via a sealed transfer vessel. These data (as tabulated in Table 1) show the state of the surface of the Mg after processing by polishing in an inert atmosphere, electrochemical stripping, or potentiostatic cycling. The data in Figure 5a show plots of the oxygen 1s binding energy region. The polished Mg foil sample shows the presence of mostly glovebox related surface contaminants, namely MgO and $MgCO_3$. The other samples contain lesser amounts of MgO, a result of removal of the initial surface oxide during electrochemical cycling. The increase in the peak around 533 eV observed for the stripped and cycled experiments, is due to an increase in oxygen containing species on the surface of the Mg foil (Mg(O)X) most likely as a result of solvent (THF) decomposition. We note that here X does not refer to a halide but rather to an unknown species. The data in Figure 5b are plots in the region of the Br 3d core level binding energy. The


DOI: 10.1021/acsami.5b04487
ACS Appl. Mater. Interfaces 2015, 7, 18406−18414

**Table 1. Core Level Binding Energies of Processed Mg Foils Measured by XPS**

| region | process | peak assignment | binding energy (eV) |
|---|---|---|---|
| O(1s) | polished | MgO | 531.2 |
| | | $MgCO_3$ | 533.2 |
| | stripped | MgO | 531 |
| | | $MgCO_3$/Mg(O)X | 533.1 |
| | cycled | MgO | 531 |
| | | $MgCO_3$/Mg(O)X | 533.2 |
| Br(3d) | polished | KLL MgO | 68.2 |
| | | Mg bulk plasmon | 71.1 |
| | | KLL Mg | 74 |
| | stripped | $MgBr_2$ | 70.7 |
| | cycled | $MgBr_2$ | 70.8 |
| Mg(2p) | polished | $Mg^0$ | 50 |
| | | MgO | 51.6 |
| | stripped | $Mg^0$ | 50.1 |
| | | $MgBr_2$/MgO | 51.6 |
| | cycled | $Mg^0$ | 50.1 |
| | | $MgBr_2$/MgO | 51.7 |

results for the stripped and cycled Mg foils show the presence of a distinct $MgBr_2$ speciation. According to one of the dissolution reactions proposed by Aurbach et al.,[40] $MgBr_2$ is a corrosion product and, because it has low solubility in THF, forms as a precipitate. As corrosion proceeds, corrosion products build up,[33] especially in the form of halide salts. Even though $MgBr_2$ accumulates during both hemispherical pitting and anisotropic pitting, the lack of nonpassivated Mg {10−10} planes upon initial stripping precludes the dismissal of $MgBr_2$ as a species contributing to the anisotropic stripping. We note that the additional peaks present in the spectra given in Figure 5b are likely due to the KLL Auger excitations of Mg and a bulk Mg plasmon (at 67.4, 73.6, and 70.0 eV respectively).[41,42] The data in Figure 5c show plots of the Mg 2p core level binding energy region. The polished Mg foil sample has peaks near where $Mg^0$ and MgO binding energies are expected. When the Mg foil is stripped or cycled, the electrolyte decomposition and corrosion products build up on the surface and the $Mg^0$ peak is reduced in intensity. Not surprisingly, the surface film formed during electrochemical processes contains mostly decomposition/corrosion products.

To further establish the character and morphology of passive films that likely mediate the anisotropic growth/dissolution behaviors established above, we used FIB in conjunction with HIM to garner a structural understanding of the films from high resolution cross-sectional images. Such images provide mechanistic insights into the process of stripping and deposition of Mg. The data in Figure 6a, c are HIM images taken at normal incidence, each showing the morphologies of typical Mg structures formed during the potentiostatic cycling (at ±500 mV, 20 cycles, for 15 min per half cycle) of a Mg foil working electrode. There are several dominant morphologies seen, including smooth areas, quasi-hexagonal symmetry crystals, and, as previously noted regarding the images presented in Figure 4, nested hexagonal motifs. The smooth areas represent nonactivated regions of the original, passivated surface of the Mg foil. Unlike previous examples, this sample processing was ended on a deposition half-cycle, resulting in many quasi-hexagonal structures with varying degrees of nesting. Two distinct quasi-hexagonal structures are evident, with apparently different degrees of filling by Mg. Each of these

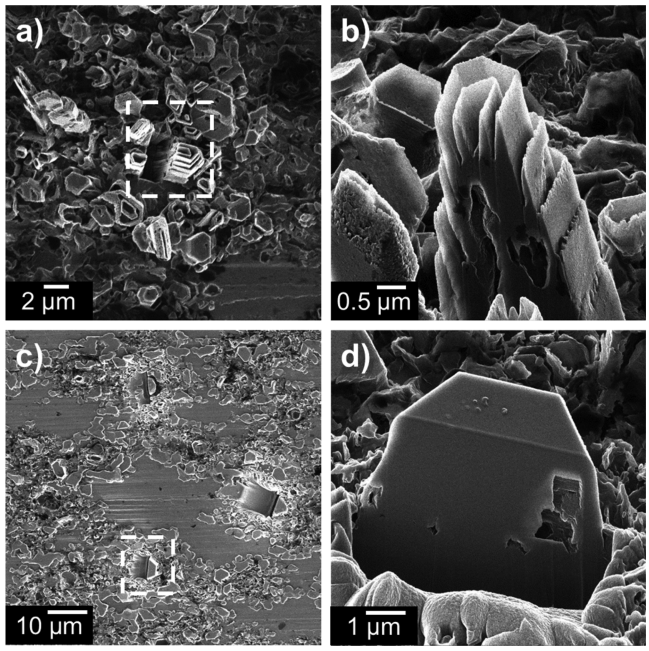


**Figure 6.** HIM images of Mg residual structures on the surface of polished Mg foil after 20 potentiostatic deposition/dissolution cycles (15 min per half cycle) at ∓500 mV. (a, c) Normal incidence view, (b, d) cross-section view at 45° in relation to a and c, respectively. Counter and reference electrodes were polished strips of Mg ribbon.

morphology types was cross-sectioned via FIB milling and imaged by HIM. The images in Figure 6b, d show views of specific cross-sections from Figure 6a, c representing the nested and non-nested structures, respectively. Figure 6b shows that the anisotropic stripping in the Grignard electrolyte often does not completely remove the Mg deposited during the previous half-cycle, as manifested in the lateral discontinuity seen at the top of the structure (combined with the relatively uniform interior) and the very thin (∼10 nm) films of oxidized material. Most notably, both cross sections reveal interstices that develop during deposition. The presence of interstices (sometimes referred to as voids or pores in literature) is common in electroplating and results from multiple grains growing into one grain to begin columnar growth.[43] As evidenced by the relatively large, uniform growth of the crystal in Figure 6d, deposition is also preferentially oriented to the {0001} plane. This deposition orientation has never been observed for EtMgBr-THF and is likely due to a combination of homoepitaxial growth and surface-oxide-limited diffusion of the Mg.

The schematic depiction given in Figure 7 illustrates several of the important features that we believe are involved in the complex growth dynamics occurring in this system. Upon initial failure of the relatively thin oxide layer formed after polishing, nucleated pit growth occurs in a relatively stochastic manner due to the localized nature of these sites and the remnants of the relatively passive surface films that remain. Switching to negative potentials initiates homoepitaxial growth on the now activated and generally {0001} textured surface planes exposed by the pits, leading to the formation of microcrystalline hexagonal motif deposits (shown here in orange). It is known that even after low potential cycling that solvent decomposition products such as γ-butyrolactone appear in the electrolyte,[19] and therefore rapid passivation from the byproducts of the


DOI: 10.1021/acsami.5b04487
ACS Appl. Mater. Interfaces 2015, 7, 18406−18414

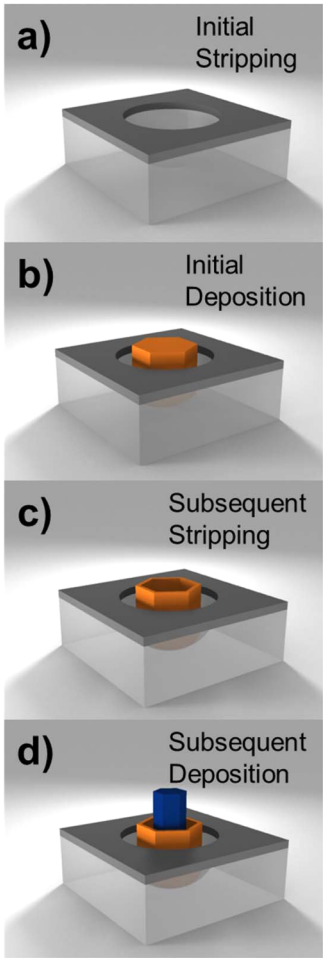


**Figure 7.** Illustrative representation of the proposed progression of the Mg surface morphology. (a) Initial stripping of the oxide layer (dark gray) leads to pitting into the substrate (light gray). (b) Deposition favors the relatively unpassivated Mg {0001} surface resulting in hexagonal crystals (orange) normal to the surface. (c) Anisotropic stripping occurs on the {0001} Mg plane of the crystal. (d) Subsequent deposition (blue) occurs within hexagonal structures forming elongated, nested residual structures.

decomposition of THF (along with $MgBr_2$) likely occurs on all Mg surfaces. Once the hexagonal passivated structures are formed, these same crystals tend to selectively strip from the substrate (Figure 7c). Other passivated surfaces become activated but are primarily localized in these and adjoining areas of the substrate. Subsequent deposition then follows upon the low overpotential, "fresh" surfaces created frequently within the residual structures from past deposition/passivation/stripping sequences. We believe that this colocalization is why we observe a progression toward unity in the ratio of deposition to dissolution in Figure 3. Initially, there is a strong overpotential for deposition due to the native passivation layer. As the potentiostatic cycling proceeds, however, stripping cycles reveal more "fresh", weakly passivated magnesium, allowing more rapid deposition. Near 100% Coulombic efficiency has been observed with EtMgBr in THF on some electrodes,[44] emphasizing the presence of an overpotential for the passivated, prismatic planes of magnesium compared to the basal plane. Extensive cycling exacerbates this effect, and as shown, causes very large 50 $\mu$m or taller columns to protrude from the electrode surface even after a relatively short sequence of cycles (Figure S8). The concern following from this, similar to issues caused by lithium metal anode dendrites,[8] is that these structures would eventually grow large enough to create an electrically active mode of failure in a full cell.

## 4. CONCLUSIONS

Passivation and corrosion processes play a crucial role in the electrochemical behavior of bulk Mg metal anodes using a nonaqueous Grignard electrolyte. Morphological characterization of the Mg working electrode after electrochemical reactions shows the formation of corrosion pits and anisotropically etched hexagonal Mg structures. Observation of the Mg working electrode after extensive deposition and dissolution cycles reveals the formation of isolated columnar structures. Although they do not have as high of an aspect ratio nor are as numerable as the dendrites formed on Li metal anodes, these structures hold the possibility of extending toward the cathode to cause battery failure as well as a potential for the loss of electroactive Mg. These results, if more broadly generalized in the electrochemistry of this metal, suggest that careful consideration of the possible anisotropy of both the deposition and the stripping of Mg is necessary for Mg to be a viable candidate for use as an anode in a rechargeable battery. Avenues of further research exist that might provide understandings of the discrete mechanisms of passive-layer formation as well as high-specificity effects of crystallographic orientation seen in deposition, passivation, and dissolution. Studies of other Mg electrolytes, ones with more complex solution equilibria and different Mg coordination spheres, will likely be needed to establish an atomistic understanding of this phenomenon and guide strategies for improving performance.

## ■ ASSOCIATED CONTENT

### Supporting Information

The Supporting Information is available free of charge on the ACS Publications website at DOI: 10.1021/acsami.5b04487.

Tabulated fit parameters for current−time transient models; CV on polished Mg foil; pit density quantitation derived from SEM micrographs; FFT; XRD diffraction patterns and polefigures; galvanostatic cycling with corresponding SEM micrograph; potentiostatic cyclings with corresponding SEM micrographs; SEM micrographs of Mg foils potentiostatically cycled for 200 cycles (PDF)

## ■ AUTHOR INFORMATION

### Corresponding Author

*E-mail: r-nuzzo@illinois.edu.

### Author Contributions

†D.J.W. and M.A.M. contributed equally to this work.

### Notes

The authors declare no competing financial interest.

## ■ ACKNOWLEDGMENTS

This work was supported as part of the Joint Center for Energy Storage Research, an Energy Innovation Hub funded by the U.S. Department of Energy, Office of Science, Basic Energy Sciences. This work was carried out in part in the Frederick Seitz Materials Research Laboratory Central Facilities, University of Illinois at Urbana−Champaign and in the Department of Physics, Bielefeld University.



DOI: 10.1021/acsami.5b04487
ACS Appl. Mater. Interfaces 2015, 7, 18406−18414

## REFERENCES


(1) Shterenberg, I.; Salama, M.; Gofer, Y.; Levi, E.; Aurbach, D. The Challenge of Developing Rechargeable Magnesium Batteries. *MRS Bull.* **2014**, *39*, 453−460.

(2) Saha, P.; Datta, M. K.; Velikokhatnyi, O. I.; Manivannan, A.; Alman, D.; Kumta, P. N. Rechargeable Magnesium Battery: Current Status and Key Challenges for the Future. *Prog. Mater. Sci.* **2014**, *66*, 1−86.

(3) Aurbach, D.; Suresh, G. S.; Levi, E.; Mitelman, A.; Mizrahi, O.; Chusid, O.; Brunelli, M. Progress in Rechargeable Magnesium Battery Technology. *Adv. Mater.* **2007**, *19*, 4260−4267.

(4) Yoo, H. D.; Shterenberg, I.; Gofer, Y.; Gershinsky, G.; Pour, N.; Aurbach, D. Mg Rechargeable Batteries: an On-going Challenge. *Energy Environ. Sci.* **2013**, *6*, 2265−2279.

(5) Xu, W.; Wang, J.; Ding, F.; Chen, X.; Nasybulin, E.; Zhang, Y.; Zhang, J.-G. Lithium Metal Anodes for Rechargeable Batteries. *Energy Environ. Sci.* **2014**, *7*, 513−537.

(6) Park, M. S.; Ma, S. B.; Lee, D. J.; Im, D.; Doo, S.-G.; Yamamoto, O. A Highly Reversible Lithium Metal Anode. *Sci. Rep.* **2014**, *4*, 3815.

(7) Jayaprakash, N.; Das, S. K.; Archer, L. A. The Rechargeable Aluminum-ion Battery. *Chem. Commun.* **2011**, *47*, 12610−12612.

(8) Yoshimatsu, I.; Hirai, T.; Yamaki, J. i. Lithium Electrode Morphology During Cycling in Lithium Cells. *J. Electrochem. Soc.* **1988**, *135*, 2422−2427.

(9) Khurana, R.; Schaefer, J.; Archer, L. A.; Coates, G. W. Suppression of Lithium Dendrite Growth Using Cross-Linked Polyethylene/Polyethylene Oxide Electrolytes: A New Approach for Practical Lithium-Metal Polymer Batteries. *J. Am. Chem. Soc.* **2014**, *136*, 7395−402.

(10) Harry, K. J.; Hallinan, D. T.; Parkinson, D. Y.; MacDowell, A. A.; Balsara, N. P. Detection of Subsurface Structures Underneath Dendrites Formed on Cycled Lithium Metal Electrodes. *Nat. Mater.* **2014**, *13*, 69−73.

(11) Schweikert, N.; Hofmann, A.; Schulz, M.; Scheuermann, M.; Boles, S. T.; Hanemann, T.; Hahn, H.; Indris, S. Suppressed Lithium Dendrite Growth in Lithium Batteries Using Ionic Liquid Electrolytes: Investigation by Electrochemical Impedance Spectroscopy, Scanning Electron Microscopy, and *in situ* $^{7}$Li Nuclear Magnetic Resonance Spectroscopy. *J. Power Sources* **2013**, *228*, 237−243.

(12) Stark, J. K.; Ding, Y.; Kohl, P. A. Nucleation of Electrodeposited Lithium Metal: Dendritic Growth and the Effect of Co-Deposited Sodium. *J. Electrochem. Soc.* **2013**, *160*, D337−D342.

(13) Mayers, M. Z.; Kaminski, J. W.; Miller, T. F., III Suppression of Dendrite Formation via Pulse Charging in Rechargeable Lithium Metal Batteries. *J. Phys. Chem. C* **2012**, *116*, 26214−26221.

(14) Lu, Z.; Schechter, A.; Moshkovich, M.; Aurbach, D. On the Electrochemical Behavior of Magnesium Electrodes in Polar Aprotic Electrolyte Solutions. *J. Electroanal. Chem.* **1999**, *466*, 203−217.

(15) Gregory, T. D.; Hoffman, R. J.; Winterton, R. C. Nonaqueous Electrochemistry of Magnesium Applications to Energy Storage. *J. Electrochem. Soc.* **1990**, *137*, 775−780.

(16) Zhu, J.; Guo, Y.; Yang, J.; Nuli, Y.; Zhang, F.; Wang, J.; Hirano, S.-i. Halogen-free Boron Based Electrolyte Solution for Rechargeable Magnesium Batteries. *J. Power Sources* **2014**, *248*, 690−694.

(17) Zhao-Karger, Z.; Mueller, J. E.; Zhao, X.; Fuhr, O.; Jacob, T.; Fichtner, M. Novel Transmetalation Reaction for Electrolyte Synthesis for Rechargeable Magnesium Batteries. *RSC Adv.* **2014**, *4*, 26924−26927.

(18) Liu, T.; Shao, Y.; Li, G.; Gu, M.; Hu, J.; Xu, S.; Nie, Z.; Chen, X.; Wang, C.; Liu, J. A Facile Approach Using $MgCl_2$ to Formulate High Performance $Mg^{2+}$ Electrolytes for Rechargeable Mg Batteries. *J. Mater. Chem. A* **2014**, *2*, 3430−3438.

(19) Barile, C. J.; Spatney, R.; Zavadil, K. R.; Gewirth, A. A. Investigating the Reversibility of in Situ Generated Magnesium Organohaloaluminates for Magnesium Deposition and Dissolution. *J. Phys. Chem. C* **2014**, *118*, 10694−10699.

(20) Cheng, Y.; Liu, T.; Shao, Y.; Engelhard, M. H.; Liu, J.; Li, G. Electrochemically Stable Cathode Current Collectors for Rechargeable Magnesium Batteries. *J. Mater. Chem. A* **2014**, *2*, 2473−2477.

(21) Bian, P.; NuLi, Y.; Abudoureyimu, Z.; Yang, J.; Wang, J. A Novel Thiolate-based Electrolyte System for Rechargeable Magnesium Batteries. *Electrochim. Acta* **2014**, *121*, 258−263.

(22) Ha, S. Y.; Lee, Y. W.; Woo, S. W.; Koo, B.; Kim, J. S.; Cho, J.; Lee, K. T.; Choi, N. S. Magnesium(II) bis(trifluoromethane sulfonyl) imide-based Electrolytes with Wide Electrochemical Windows for Rechargeable Magnesium Batteries. *ACS Appl. Mater. Interfaces* **2014**, *6*, 4063−4073.

(23) Doe, R. E.; Han, R.; Hwang, J.; Gmitter, A. J.; Shterenberg, I.; Yoo, H. D.; Pour, N.; Aurbach, D. Novel, Electrolyte Solutions Comprising Fully Inorganic Salts with High Anodic Stability for Rechargeable Magnesium Batteries. *Chem. Commun.* **2014**, *50*, 243−245.

(24) Benmayza, A.; Ramanathan, M.; Arthur, T. S.; Matsui, M.; Mizuno, F.; Guo, J.; Glans, P.-A.; Prakash, J. Effect of Electrolytic Properties of a Magnesium Organohaloaluminate Electrolyte on Magnesium Deposition. *J. Phys. Chem. C* **2013**, *117*, 26881−26888.

(25) Muldoon, J.; Bucur, C. B.; Oliver, A. G.; Zajicek, J.; Allred, G. D.; Boggess, W. C. Corrosion of Magnesium Electrolytes: Chlorides − the Culprit. *Energy Environ. Sci.* **2013**, *6*, 482.

(26) Zhao-Karger, Z.; Zhao, X.; Fuhr, O.; Fichtner, M. Bisamide Based Non-nucleophilic Electrolytes for Rechargeable Magnesium Batteries. *RSC Adv.* **2013**, *3*, 16330−16335.

(27) Guo, Y.-s.; Zhang, F.; Yang, J.; Wang, F.-f.; NuLi, Y.; Hirano, S.-i. Boron-based Electrolyte Solutions with Wide Electrochemical Windows for Rechargeable Magnesium Batteries. *Energy Environ. Sci.* **2012**, *5*, 9100−9106.

(28) Zhang, R.; Yu, X.; Nam, K.-W.; Ling, C.; Arthur, T. S.; Song, W.; Knapp, A. M.; Ehrlich, S. N.; Yang, X.-Q.; Matsui, M. $\alpha$-$MnO_2$ as a Cathode Material for Rechargeable Mg Batteries. *Electrochem. Commun.* **2012**, *23*, 110−113.

(29) Yagi, S.; Tanaka, A.; Ichikawa, Y.; Ichitsubo, T.; Matsubara, E. Electrochemical Stability of Magnesium Battery Current Collectors in a Grignard Reagent-Based Electrolyte. *J. Electrochem. Soc.* **2013**, *160*, C83−C88.

(30) Souto, R. M.; González, S.; Salvarezza, R. C.; Arvia, A. J. Kinetics of Copper Passivation and Pitting Corrosion in $Na_2SO_4$ Containing Dilute NaOH Aqueous Solution. *Electrochim. Acta* **1994**, *39*, 2619−2628.

(31) Shibata, T.; Takeyama, T. Pitting Corrosion as a Stochastic Process. *Nature* **1976**, *260*, 315−316.

(32) Tunold, R.; Holtan, H.; Berge, M.-B. H.; Lasson, A.; Steen-Hansen, R. The Corrosion of Magnesium in Aqueous Solution Containing Chloride Ions. *Corros. Sci.* **1977**, *17*, 353−365.

(33) Thomas, S.; Medhekar, N. V.; Frankel, G. S.; Birbilis, N. Corrosion Mechanism and Hydrogen Evolution on Mg. *Curr. Opin. Solid State Mater. Sci.* **2015**, *19*, 85−94.

(34) Hill, C. L.; Vander Sande, J. B.; Whitesides, G. M. Mechanism of Formation of Grignard Reagents. Corrosion of Metallic Magnesium by Alkyl Halides in Ethers. *J. Org. Chem.* **1980**, *45*, 1020−1028.

(35) McCall, C.; Hill, M.; Lillard, R. Crystallographic Pitting in Magnesium Single Crystals. *Corros. Eng., Sci. Technol.* **2005**, *40*, 337−343.

(36) Liu, M.; Qiu, D.; Zhao, M.-C.; Song, G.; Atrens, A. The Effect of Crystallographic Orientation on the Active Corrosion of Pure Magnesium. *Scr. Mater.* **2008**, *58*, 421−424.

(37) Song, G.-L.; Xu, Z. Effect of Microstructure Evolution on Corrosion of Different Crystal Surfaces of AZ31 Mg Alloy in a Chloride Containing Solution. *Corros. Sci.* **2012**, *54*, 97−105.

(38) Shin, K. S.; Bian, M. Z.; Nam, N. D. Effects of Crystallographic Orientation on Corrosion Behavior of Magnesium Single Crystals. *JOM* **2012**, *64*, 664−670.

(39) Lillard, R. S.; Wang, G. F.; Baskes, M. I. The Role of Metallic Bonding in the Crystallographic Pitting of Magnesium. *J. Electrochem. Soc.* **2006**, *153*, B358−B364.

(40) Aurbach, D.; Moshkovich, M.; Schechter, A.; Turgeman, R. Magnesium Deposition and Dissolution Processes in Ethereal Grignard Salt Solutions Using Simultaneous EQCM-EIS and In Situ FTIR Spectroscopy. *Electrochem. Solid-State Lett.* **2000**, *3*, 31−34.




DOI: 10.1021/acsami.5b04487
*ACS Appl. Mater. Interfaces* 2015, 7, 18406−18414

(41) Fuggle, J. C.; Watson, L. M.; Fabian, D. J.; Affrossman, S. X-ray Excited Auger and Photoelectron Spectra of Magnesium, Some Alloys of Magnesium and its Oxide. *J. Phys. F: Met. Phys.* **1975**, *5*, 375−383.
(42) Kurth, M.; Graat, P. C. J. Quantitative Analysis of the Plasmon Loss Intensities in X-ray Photoelectron Spectra of Magnesium. *Surf. Interface Anal.* **2002**, *34*, 220−224.
(43) Abys, J. A., Palladium Electroplating. In *Modern Electroplating*; John Wiley & Sons: New York, 2010; pp 327−368.
(44) Liebenow, C.; Yang, Z.; Lobitz, P. The Electrodeposition of Magnesium Using Solutions of Organomagnesium Halides, Amidomagnesium Halides and Magnesium Organoborates. *Electrochem. Commun.* **2000**, *2*, 641−645.



DOI: 10.1021/acsami.5b04487
*ACS Appl. Mater. Interfaces* 2015, 7, 18406−18414